Journal of Sound and Vibration 645 (2026) 120124

Contents lists available at ScienceDirect

Journal of Sound and Vibration

journal homepage: www.elsevier.com/locate/jsvi

Wave propagation in beam-like in-vacuo tuneable structured fabrics

Davide Raffaele [a], Emiliano Rustighi [a,*], Paolo Gardonio [b], Ciro Malacarne [c], Matteo Perini [c]

[a] Department of Industrial Engineering, University of Trento, Italy
[b] Polythecnic Department of Engineering and Architecture, University of Udine, Udine, Italy
[c] ProM Facility, Trentino Sviluppo S.p.A, Rovereto, Italy

ARTICLE INFO

Keywords:
Structured fabrics
Wave propagation
Vacuum-tuneable waveguides
Smart materials
Dispersion curves

ABSTRACT

In-vacuo tuneable structured fabrics represent an innovative class of smart materials capable of modulating their mechanical and dynamic properties through controlled confinement pressure. When arranged in beam-like configurations, these structures can operate as vacuum-controlled waveguides with pressure-dependent stiffness and dispersion characteristics. This paper presents a preliminary investigation of elastic wave propagation in a beam-like vacuum-controlled tuneable structured fabrics under variable confinement pressures. A prototype was designed and fabricated to assess both the technical feasibility and manufacturability. Experiments were conducted using a correlation-based wavenumber identification technique to characterise wave behaviour. A one-dimensional wave finite element model was implemented in COMSOL Multiphysics, employing Floquet boundary conditions and Hertzian contact theory with a scaling factor to account for contact multiplicity. Computed dispersion curves at 20 kPa and 80 kPa confinement pressures show qualitative agreement with experimental measurements. Results demonstrate that increasing confinement pressure enhances structural stiffness and shifts dispersion branches toward higher frequencies. Wave mode shape analysis confirms multiple bending and longitudinal modes consistent with classical beam theory. These findings suggest that in-vacuo structured fabrics could provide a new means for the development of programmable metamaterials for vibration control.

1. Introduction

In recent years, research on composite materials has increasingly focused on innovative core architectures and sandwich configurations that provide enhanced mechanical and functional performance [1–5], particularly for vibration attenuation and noise suppression applications [6–8]. Among these developments, structured fabrics — lattice-like assemblies composed of rigid truss elements — have emerged as promising primary candidates for sandwich composites owing to their tuneable stiffness and damping properties, which are often facilitated by advances in additive manufacturing technologies [9,10]. When encased within vacuum-sealed skins, these fabrics can exhibit remarkable variations in their mechanical response. Wang et al. [11] demonstrated that chain mail-like structures subjected to a vacuum pressure of 90 kPa achieved stiffness enhancements exceeding 25 times those of their unconfined

* Corresponding author.
E-mail address: emiliano.rustighi@unitn.it (E. Rustighi).

https://doi.org/10.1016/j.jsv.2026.120124
Received 12 March 2026; Received in revised form 1 September 2026; Accepted 7 September 2026
Available online 8 September 2026
0022-460X/© 2026 Published by Elsevier Ltd.

state, stimulating extensive research into their adaptive behaviour [11–13]. Rustighi et al. [6] further showed that their vibration responses can be modulated through vacuum-level adjustment, with cubic geometries exhibiting the highest bending stiffness. Building on these findings, some studies explored the feasibility of employing vacuum-sealed structured fabrics as Tuneable Vibration Absorbers (TVAs) [7,8].

The mechanical behaviour of these systems is inherently associated with jamming phenomena [14–16], where particle aggregation under a confinement pressure leads to increased compressive resistance and structural locking [6,7,11]. Unlike granular media, structured fabrics exploit both convex and non-convex contact interactions, achieving greater compressive strength while retaining tensile load-bearing capability [17,18]. Contact mechanics therefore plays a central role in their tuneable behaviour, enabling controlled variations in bending stiffness that are particularly advantageous for adaptive vibration control. Indeed, beam-like TVAs incorporating structured fabrics have demonstrated resonance frequency modulation governed by vacuum pressure adjustment without significant degradation of damping performance [7,8,19–21]. Despite the growing interest in their quasi-static and vibrational response, the wave propagation characteristics of vacuum-sealed structured fabrics under varying confinement pressures remain unexplored. Understanding elastic wave propagation in these media and its dependence on vacuum pressure is essential for predicting their dynamic behaviour, identifying band gaps, and optimising their design for vibration control and acoustic insulation.

Wave propagation and band-gap formation in contact-based periodic systems have attracted considerable attention in recent years. In particular, Boechler et al. [22] demonstrated that one-dimensional diatomic granular crystals with three-particle unit cells exhibit tuneable vibrational band gaps, whose frequency range can be adjusted by varying the static pre-compression acting on the Hertzian contacts. Extending these concepts to higher-dimensional systems, Manjunath et al. [23] investigated plane-wave propagation in two- and three-dimensional monodisperse periodic granular media, highlighting the influence of the contact network on the dispersion characteristics. Göncü et al. [24] demonstrated that phononic band gaps can be tuned through mechanically induced pattern transformations. Specifically, uniaxial compression causes stiff particles, initially separated by soft silicone-rubber cylinders, to come into direct contact, thereby altering the contact configuration and providing an effective mechanism for adaptive wave manipulation.

While tuneable wave propagation and band-gap formation have been extensively investigated in granular crystals and other periodic contact-based systems, these phenomena have not yet been explored in vacuum-sealed structured fabrics, where pressure-dependent contact mechanics offers new opportunities for tailoring dynamic responses. Therefore, this study aims to investigate, for the first time, the propagation of elastic waves within vacuum-sealed structured fabrics subjected to different confinement pressures, providing new insights into their potential for tuneable vibration control and acoustic insulation applications.

Wave propagation in elastic waveguides has traditionally been analysed using analytical formulations or matrix-based techniques. However, these approaches become impractical for complex geometries and inhomogeneous materials [25–27]. Numerical techniques based on the Finite Element Method (FEM) effectively address these limitations by discretising the domain and assembling the corresponding global equilibrium equations. Nevertheless, conventional three-dimensional FEM analysis remain computationally demanding for large-scale or high-frequency problems, as fine meshes are required to accurately capture short wavelengths. To mitigate these limitations, alternative techniques such as the Boundary Element Method (BEM), Finite Difference Method (FDM), and Wave Finite Element (WFE) method have been developed. As discussed in [28], each approach presents distinct advantages and drawbacks for modelling guided-wave phenomena. Among them, the WFE method is particularly attractive because it combines FEM discretisation with a wave-based formulation [29]. An efficient implementation of the WFE method employs Floquet–Bloch theory within a standard finite element framework to analyse periodic structures. The Floquet Boundary Condition (Floquet BC) method further reduces computational cost by restricting the analysis to a single unit cell subject to boundary conditions derived from elasto-dynamic and periodicity principles. Applications of Floquet BCs to periodic waveguides are well documented in the literature [30,31]. In this work, the in-vacuo structured fabrics are modelled using the Floquet BC method implemented in COMSOL Multiphysics [32]. Using this approach, this study marks a first attempt to model wave propagation in the context of tuneable structured fabrics. Simplifying assumptions are also introduced to account for the complex influence of confinement pressure.

The numerical results are then validated experimentally through a wavenumber identification approach. Wavenumber identification methods are widely employed both to verify numerical simulations and to reveal physical phenomena that may not fully captured by models. Various techniques have been proposed in the literature, including the spatial Discrete Fourier Transform (DFT) [33], Prony analysis [34], sparse iterative methods [35], and laser-ultrasonic techniques [36]. Among the simplest approaches, the phase-difference method [37,38] estimates the wavenumber from the phase shift between responses measured at adjacent locations. To improve accuracy, the signals are typically windowed to exclude reflections, while sensors are positioned sufficiently far from both boundaries and excitation sources. A modified acoustic-based technique was introduced in [39] for the structural vibration analysis of pipes under anechoic conditions, where three equally spaced accelerometers were used to estimate the wavenumber from transfer function relationships. To address the inherent limitations of such methods, Ferguson et al. [40] developed a correlation-based approach for two-dimensional structures by correlating measured Frequency Response Functions (FRFs) with trial wavefields. Although this technique identifies only real wavenumbers, thus neglecting near-field and damping effects, it showed better agreement with theoretical predictions than two-dimensional spatial DFTs and was subsequently extended to one-dimensional systems such as cables and beams [41,42].

In summary, this paper presents a preliminary experimental and numerical investigation of wave propagation in beam-like, vacuum-controlled structured fabrics under varying confinement pressures. The paper is organised as follows. Section 2 describes the in-vacuo composite structure employed in this work. Section 3 describes the experimental setup for wave propagation measurements, introduces the correlation-based wavenumber identification technique, and analyses the experimental data, highlighting the influence of vacuum pressure on the material dynamic response. Section 4 presents a one-dimensional WFE model of the composite structure, whose dispersion curves are validated against the experimental results. The corresponding wave mode shapes are then examined to

illustrate the wave behavior. This combined experimental and numerical approach provides a comprehensive understanding of wave propagation in these vacuum-tuneable fabrics. Finally, Section 5 summarises the main findings and conclusions of the study.

2. Beam-like in-vacuo structured fabrics: design, fabrication, and packaging

The experimental investigation presented in this work required the fabrication of a single-span beam-like structured fabric approximately 3.6 m long. Such a specimen considerably exceeds the build volume of conventional additive manufacturing systems and therefore represents a significant manufacturability challenge. Consequently, before describing the structural architecture of the material, it is important to illustrate the adopted manufacturing strategy, since it constitutes a key enabling step for the realisation of the experimental prototype.

The structured fabric was manufactured in Nylon PA12 using an HP Multi Jet Fusion (MJF) 3D 4200 printer [43], featuring a build volume of $380 \times 284 \times 380$ mm. As a powder-bed fusion process, MJF uses unfused powder to support the component during fabrication, thereby eliminating the need for dedicated support structures. These characteristics make MJF particularly suitable for manufacturing highly interconnected articulated structures, which would be difficult to fabricate using alternative additive manufacturing technologies such as fused deposition modelling (FDM) or stereolithography (SLA). Since the printer build volume is considerably smaller than the required specimen length, the structured fabric was printed as a single continuous component in a coiled (rolled-up) configuration, allowing the entire specimen to fit within the available build envelope without introducing joints or discontinuities. Using CAD software, a two-dimensional spiral geometry was first defined to establish the coiled path, after which the elementary cells were patterned with a prescribed pitch to maintain the minimum gap between neighbouring cells. The geometry was then replicated along the vertical direction to obtain the required specimen height. After printing, the specimen was removed from the powder bed through a two-stage de-powdering procedure. First, the printer automated recovery system removed most of the unfused powder using a suction system, allowing the material to be recycled for subsequent production. The remaining powder was then removed manually by carefully unfolding the specimen and cleaning it by glass-bead sandblasting to eliminate residual powder trapped within the lattice. This procedure released all articulated unit cells while preserving the continuity of the structure, since no assembly or post-print joining operations were required. Consequently, no geometric discontinuities were introduced that could influence either the wave propagation measurements or the comparison with the idealised numerical model.

Fig. 1 illustrates the complete manufacturing process together with the final beam-like specimen. Figs. 1(a) and 1(b) show the CAD model of the coiled printing layout and the fabricated specimen after unfolding and de-powdering, respectively, whereas Figs. 1(c) and 1(d) present the octahedra-sphere unit-cell geometry and the corresponding specimen after packaging within the vacuum bag.

As discussed in the introduction, the vacuum-controlled tuneable structured fabric considered in this work consists of rigid truss-

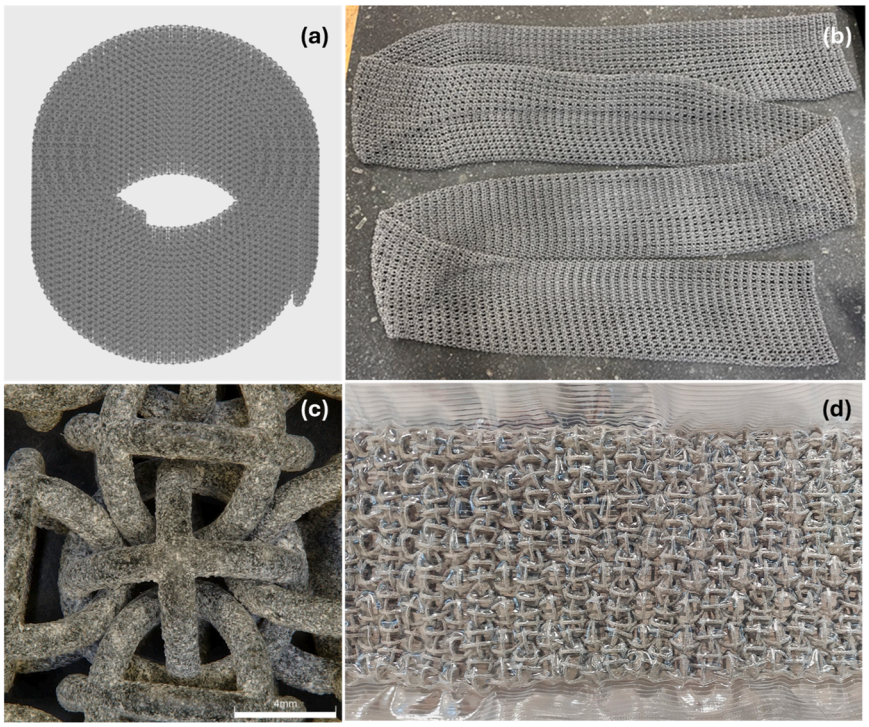

Fig. 1. Manufacturing, architecture and packaging of the beam-like in-vacuo structured fabric. (a) CAD model of the coiled printing layout adopted to fit the complete specimen within the printer build volume; (b) fabricated specimen after unfolding and de-powdering; (c) 3D microscope image of the octahedra-sphere unit cells; (d) fabricated specimen enclosed within the vacuum bag after packaging.

like unit elements interconnected to each other to create loose chain mails. Several structured fabric architectures can be designed, depending on both the geometry of the rigid unit elements and the lattice organisation of the particles themselves [3,6]. In a recent study conducted by some of the authors [44], three particle geometries, namely octahedra, octahedra-spheres and cubes, were investigated to assess the influence of granular jamming on the bending stiffness. Multiple overlapping fabric layers were also considered to evaluate the effect of layer jamming. The choice of the specimen's macroscopic and mesoscopic dimensions, as well as the applied pressure range, is based on this comparative experimental investigation. In the present work, hence, a single-layer fabric composed of octahedra-sphere particles was selected to provide a representative beam-like configuration for the investigation of elastic wave propagation.

The octahedra-sphere particles are organised in a lattice with connecting directions at 90°. Each particle has a nominal size of 10 mm and is composed of curved truss members having a circular cross-section of approximately 1 mm in diameter. To obtain the jammed configuration, the structured fabric was enclosed within a vacuum bag and hermetically sealed along its edges using a heat-sealing press, as shown in Fig. 1(d). The application of vacuum generated the confinement pressure required to jam the interconnected unit cells, transforming the initially compliant fabric into a beam-like structure suitable for the experimental investigation.

Under the isostatic compression imposed by the vacuum bag, the chain mail partially retains its original lattice organization. Consequently, the in-vacuo composite cannot be classified either as a fully amorphous material or as a perfectly periodic lattice. Rather, it may be regarded as a quasi-amorphous or quasi-crystalline solid, depending on whether emphasis is placed on the jammed internal configuration or on the underlying chain-mail architecture. This combination of disordered and lattice-like characteristics provides the material with low density and high mechanical performance. From a wave propagation viewpoint, this observation is particularly important because it justifies the modelling strategy adopted in the following sections. Although the local contact network evolves under confinement pressure and exhibits a certain degree of disorder, the underlying lattice organisation remains sufficiently regular for the jammed structure to be approximated as an equivalent periodic medium. This approximation forms the basis of the Wave Finite Element model developed in Section 4 to characterise the pressure-dependent dispersion behaviour of the structured fabric.

3. Experimental characterization of dispersion properties

This section presents the experimental results on wave propagation in the in-vacuo tuneable structured fabrics described herein. The results were obtained using a correlation-based wavenumber identification technique and serve as a reference for validating the numerical findings reported in Section 4. The experimental tests were conducted at vacuum pressures of 20 and 80 kPa, enabling a clear comparison of the effect of vacuum level on the material dynamic response. The experimental setup is first described, followed by the corresponding experimental results.

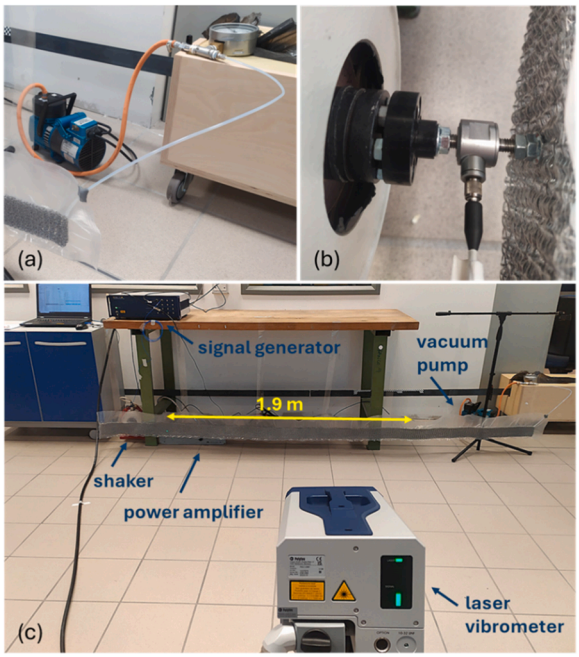

Fig. 2. Wave propagation setup for the beam-like in vacuum composite structure: (a) vacuum systems, (b) attachment of the force gauge to the composite structure, and (c) test rig used for the measurements.

3.1. Experimental setup

A series of vacuum-controlled vibration experiments were performed to characterise the dynamic response of the structured fabric under given boundary and loading conditions. The experimental procedure comprised (i) deflation of the enclosing plastic bag to establish an in-vacuo configuration and (ii) excitation and response measurements using an electrodynamic shaker and a scanning laser vibrometer.

To achieve the in-vacuo condition, the structured fabric was enclosed in a plastic bag and deflated using a small suction pipe inserted through a small opening, which was subsequently sealed to ensure airtightness. As shown in Fig. 2(a), the suction pipe was connected to a diaphragm vacuum pump (KNF NEUBERGER UN726 TTP) through an analogue vacuum meter (RS PRO 188-986) and a check valve. Under vacuum conditions, the structured fabric measured approximately 3.3 m in length and 0.08 m in width.

Vibration measurements were then conducted on the structured fabric under vacuum. The specimen was suspended at multiple points along its length using adhesive tape strips, as illustrated in the full experimental setup in Fig. 2(c). The structure was excited using an electro-dynamic shaker (LDS V406) driven by a power amplifier (LDS PA100E). The shaker, Fig. 2(b), was coupled to the central region of the composite structure via a force sensor (Dytran 1051V2), which was bonded to the surface to prevent damage to the fragile plastic skin and to ensure a stable connection throughout the experiments. Several excitation configurations were evaluated during preliminary testing and produced consistent dynamic responses within the experimental uncertainty. The selected configuration was therefore adopted as it provided reliable coupling while preserving the integrity of the plastic enclosure. To ensure that the response remained within the linear regime about the preloaded contact state, the excitation level was intentionally kept as low as possible, corresponding to a force power spectral density (PSD) of −55 dB relative to 1 N^2/Hz. Under these conditions, the measured coherence remained high up to approximately 5–6 kHz.

Excitation was generated using the internal signal generator of the PSV Scanning Vibrometer (Polytec QTec PSV-500) in the form of a periodic chirp spanning the frequency range from 0 to 10 kHz. Data acquisition was performed with an FFT bandwidth of 10 kHz, 3200 FFT lines, a sampling frequency of 25 kHz, and a record length of 320 ms, corresponding to a frequency resolution of 3.125 Hz. The excitation signal was applied continuously as consecutive periodic chirps with no time interval between successive records. Within the PSV acquisition software, the periodic chirp is implemented as a Schroeder-phased multisine, i.e. a discrete sum of harmonically related sinusoids with a quadratic phase distribution [45,46]. This approach combines the low crest factor and high energy injection of a continuous frequency sweep with the leak-free, periodic properties of a multisine, making it ideal for high-SNR laser Doppler vibrometry measurements without the need for windowing.

Structural responses were acquired using the laser scanning vibrometer at an array of measurement points located sufficiently far from the free ends to avoid near-field effects, and transfer functions were computed using the integrated software. At each scan point, the mobility FRF was obtained by averaging three consecutive acquisitions, thereby improving the signal-to-noise ratio. Details of measurement grid are provided in Section 3.3. Repeatability was assessed by conducting multiple tests over different vacuum cycles. Following each change in confinement pressure, sufficient time was allowed for stabilisation before data acquisition, and the vacuum pressure was continuously monitored throughout each test to ensure that the prescribed confinement level was maintained. Additional verification procedures included checks of the specimen's vertical alignment along its length and monitoring of the confinement pressure during each test. Although minor local effects associated with the adhesive supports, force sensor attachment, and plastic membrane cannot be completely excluded, their influence was considered limited compared with the dominant effect of the confinement pressure on the dispersion behaviour.

3.2. Correlation technique

A correlation-based wavenumber identification technique for wavenumber estimation in two-dimensional (2D) structures was proposed by Ferguson et al. [40]. The approach involves computing, for each frequency, the correlation between FRF measurements and a wavefield derived from trial wavenumbers of travelling waves propagating in two orthogonal directions. With appropriate

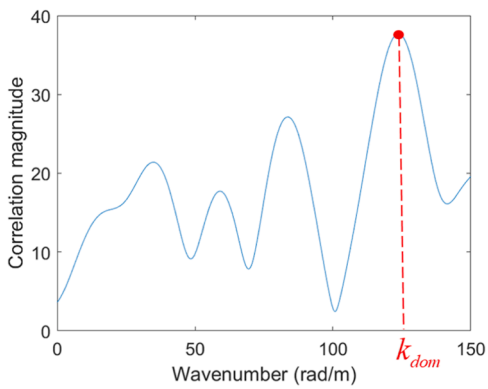

Fig. 3. Example of correlation magnitude versus trail wavenumbers at an arbitrary frequency value.

modifications, the same principle can be extended to one-dimensional (1D) structures. For discrete measurements, the formulation of the correlation technique for a single wave in a 1D waveguide can therefore be expressed as

$$\widehat{W}(k_{tz},\omega) \cong \left(\frac{l_z}{N}\right)\sum_{i=1}^{N} w^*(z_i,\omega)\mathrm{e}^{-\mathrm{j}k_t z_i} \tag{1}$$

where $\widehat{W}(k_{tz},\omega)$ is the correlation coefficient evaluated at a trial wavenumber k_t and angular frequency ω, z_i is the spatial location of the array at which the responses $w(z_i,\omega)$ are measured, l_z is the length of the spatial array, N is the number of discrete measurement locations, $\mathrm{j}=\sqrt{-1}$ is the imaginary unitary number and $()^*$ indicates the complex conjugate operator.

For each frequency, the correlation function exhibits peak values at specific trial wavenumbers. The wavenumber corresponding to the highest peak is extracted at each frequency step to construct the dispersion curves. As an example, Fig. 3 presents a typical wavenumber-correlation magnitude plane obtained from Eq. (1) at an arbitrary frequency, showing the dominant wavenumber k_{dom} (highlighted in red) and three additional dominant wavenumbers with decreasing correlation magnitude.

Compared to other experimental techniques such as the phase-difference method [37,38], the correlation approach enables the use of an arbitrary number of measurement points for wavenumber estimation, without the requirement of equal spacing. However, the method is limited to the identification of real wavenumbers (i.e., travelling waves) and therefore cannot capture near-field effects or material damping associated with complex wavenumbers. To address this limitation, several extensions of the correlation technique have been proposed, including the method by Ichchou et al. [47], which enables the estimation of complex wavenumbers and thus accounts for near-field effects and material damping. Nevertheless, in the present work, the standard correlation technique was adopted for its computational efficiency and robustness, as the primary focus remains on far-field wave propagation and cut-off frequencies identification, where the contribution of near-field effects and damping is negligible. This choice is also consistent with the scope of the numerical study, which focuses on the identification of real wavenumbers.

3.3. Experimental dispersion curves under variable vacuum levels

In the following are presented the measured dispersion curves, in the form of wavenumber against frequency, obtained for the in-vacuo tuneable structured fabrics via the correlation technique. The frequency response functions used in the dispersion analysis were obtained under the excitation conditions described in Section 3.1. To maximise the number of measurements and thus improve the accuracy of the wavenumber estimation, 717 measurement points were acquired with a sensor spacing of 0.0027 m, resulting in a spatial array length of 1.9 m. As shown in Fig. 2(c), the measurements were conducted at a sufficient distance from both the shaker and the free ends (approximately 20 cm from the shaker and 80 cm from the opposite free end) to avoid near-field effects. Trial wavenumbers were subsequently evaluated over the range 0-314 rad/m with a wavenumber step of 0.1 rad/m. The chosen temporal and spatial parameters ensured the exclusion of both temporal and spatial aliasing. To eliminate noisy data and increase readability, only the results up to 5 kHz are shown.

Fig. 4 shows the experimental dispersion curves obtained under a vacuum pressure of 20 kPa. In particular, Fig. 4(a) shows a colour map of the correlation magnitude in the wavenumber-frequency plane, obtained through the three-dimensional function defined in Eq. (1). As indicated by the colour bar, the correlation magnitude ranges from blue (lowest values) to yellow (highest values). Several streaks are visible in the color map, indicating the presence of multiple propagating wave modes in the investigated frequency range. In

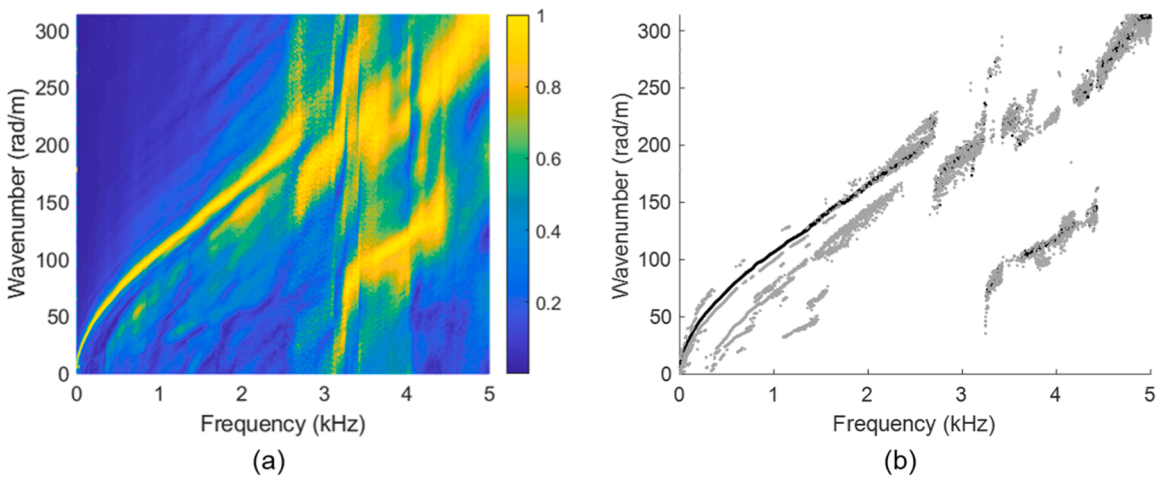

Fig. 4. Experimental dispersion curves for the structured fabrics with a vacuum pressure of 20 kPa obtained using the correlation method. (a) colormap of the correlation magnitude at the wavenumber-frequency plane from the highest value (in yellow) to the lowest (in blue), (b) dominant wavenumber (black), and three other dominant wavenumbers with decreasing correlation magnitude (grey).

Fig. 4(b), to highlight these modes, the dominant wavenumber at each frequency is plotted in black, while three additional less-dominant wavenumbers with decreasing correlation magnitude are plotted in grey. At first glance, all wave modes appear dispersive, similar to flexural modes in beams; however, the detailed numerical analysis presented in the next section will provide deeper insights into their characteristics.

A notable feature is observed at approximately 2.6 kHz, where the dominant dispersion branch exhibits a change in curvature, indicating a variation in phase velocity. This behavior suggests a possible wave mode transition, such as mode veering, or the presence of wave modes with negative group velocity components. Beyond this frequency, higher-order branches become more pronounced, indicating the onset of additional propagating modes and an increase in modal density. Moreover, some branches appear only above specific frequencies, indicating cut-off frequencies associated with higher-order modes, while the absence of certain branches at lower frequencies suggests that these modes cannot propagate below their respective cut-off conditions. Finally, the figures show no band gaps within the investigated frequency range.

Fig. 5 shows the corresponding dispersion curves obtained at a vacuum level of 80 kPa. Compared with the 20 kPa results in Fig. 4, these curves exhibit a lower slope and a rightward shift, indicating an increase in structural stiffness associated with the higher vacuum level. Similarly, a distinct feature is observed at approximately 3.2 kHz, where the dominant branch shows an apparent change in curvature and interaction with secondary branches, suggesting a wave mode transition or the presence of negative group velocity components. In addition, fewer cut-on frequencies are observed than in the 20 kPa case, while higher-order branches are more clearly separated.

It is worth noting that the wavenumbers estimated using the correlation technique account only for their real component. Therefore, despite the careful experimental procedures implemented to minimise their influence, the estimated wavenumbers may still be affected by near-field wave contributions associated with boundary reflections, source positioning, and material damping. Moreover, the coexistence of multiple wavenumbers further increases the complexity of their estimation.

4. Numerical modelling and dispersion examination

This section presents a numerical analysis of wave propagation in vacuum-controlled tuneable structured fabrics. First, a WFE model of the composite structure is introduced, and the resulting dispersion curves are compared with the experimental data presented above. Next, wave mode shapes are analysed, and the numerical dispersion curves are compared with analytical Euler-Bernoulli beam solutions to illustrate the physical wave behaviour.

4.1. WFE model of the in-vacuo TSF

As mentioned in the introduction, one of the most widely used methods for determining the dispersion curves of a periodic waveguide is the WFE method [29], implemented in COMSOL Multiphysics via the Floquet BCs [32]. This method requires discretising only a representative portion of the waveguide of thickness S, which captures its periodicity, and applying a geometric assumption (i.e., waveguide periodicity) to the problem domain through the following Floquet BC equation:

$$\mathbf{u}_{dst} = \mathbf{u}_{src}\, e^{-i\, \mathbf{k}_F (\mathbf{r}_{dst} - \mathbf{r}_{src})}, \tag{2}$$

where $\mathbf{u}$ denotes the displacement field vector, and subscripts *"dst"* and *"src"* designate a variable defined at the destination and the

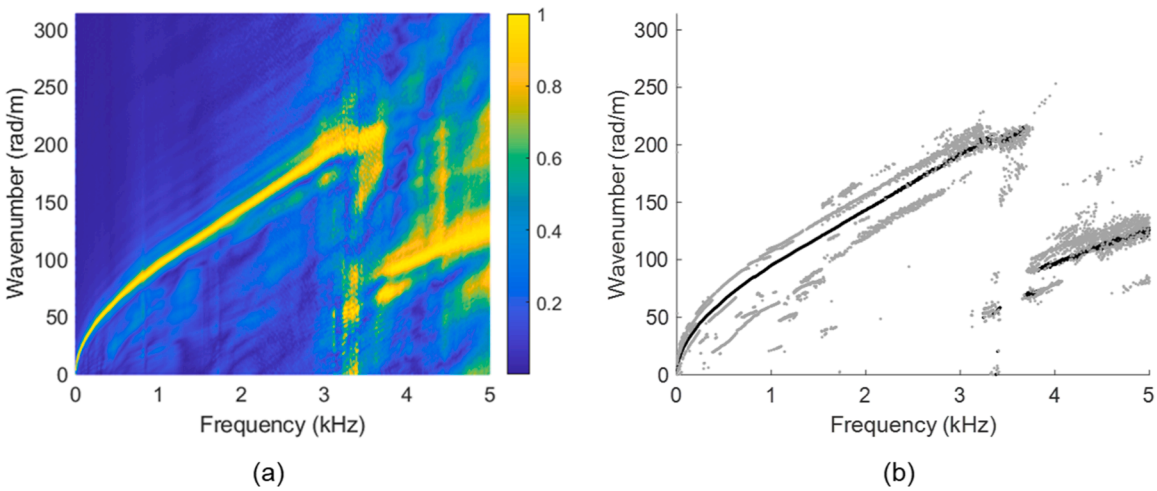

Fig. 5. Experimental dispersion curves for the structured fabrics with a vacuum pressure of 80 kPa obtained using the correlation method. (a) colormap of the correlation magnitude at the wavenumber-frequency plane from the highest value (in yellow) to the lowest (in blue), (b) dominant wavenumber (black), and three other dominant wavenumbers with decreasing correlation magnitude.

source boundaries, respectively. $\mathbf{k}_F$ is the Floquet wavenumber vector, defined in the Cartesian coordinates, and $\mathbf{r}$ represents the spatial coordinates vector of the boundaries on which the condition is applied [32]. This condition enforces that the displacement field on one periodic boundary differs from that on the opposite boundary only by a complex phase shift, governed by the Floquet wavenumber, thereby allowing wave propagation in an effectively infinite periodic structure to be modelled using a single unit cell.

In COMSOL Multiphysics, the eigenfrequency analysis under Floquet BCs is performed by first defining the unit cell geometry and assigning the Floquet periodicity to the relevant boundaries. The Floquet wavenumber is treated as a user-defined parameter, and a parametric sweep is performed to compute the eigenfrequencies at each wavenumber. These results are then used to construct the dispersion curves, efficiently capturing the band structure without modelling multiple unit cells. However, a phenomenon to consider when using these boundary conditions is the so-called band folding; that is, these dispersion curves become periodic with respect to wavenumber, with the first Brillouin zone $\left(\frac{-\pi}{S} < k < \frac{\pi}{S}\right)$ usually sufficient for analysis, while additional folding arises if the chosen problem domain is larger than the smallest repeatable one [32,48]. As described in Section 2, the structured fabrics investigated in this work consist of octahedral spheres formed by rigid, truss-like elements interconnected in a lattice. These elements exhibit non-linear contact stiffness, which often induces numerical convergence challenges [49]. To address this issue, the simplified beam model shown in (Fig. 6(a)) was employed. The model must capture the essential features of the real structured fabric, particularly the contact mechanics between octahedral spheres and their effective stiffness and mass properties. It comprises eight hollow spheres, each connected through four contact points. Notably, the number of spheres was established to represent the effective beam width under vacuum conditions. They are uniformly distributed, reflecting the quasi-lattice-like architecture of the tuneable structured fabric. The beam is assumed to extend infinitely along the z-axis, with unit cells (see Fig. 6(b)) defined by an outer diameter of 10 mm and a wall thickness of 1 mm. Consequently, the term $\mathbf{r}_{dst} - \mathbf{r}_{src}$ in Eq. (2) corresponds to the distance between parallel faces, S, which is equal to the outer diameter. Free boundary conditions are automatically applied to all remaining boundaries. Any contribution of the plastic skin's bending stiffness was considered negligible and is therefore not included in the model.

The key feature that the simplified model must incorporate is the inter-element contact, specifically between octahedral spheres [49]. These contacts are critical, as they govern the macroscopic mechanical behaviour of the structured fabric. They are induced by the confinement pressure applied via the fabric airtight bag. As the vacuum pressure increases, both the number of contact points and the contact area per sphere increase, directly influencing the global stiffness of the material. Although the real contact network is inherently heterogeneous due to local rearrangements of the chain-mail architecture during jamming, the structured fabric retains an underlying periodic organisation, allowing the contact behaviour to be represented through an equivalent periodic unit cell. In fact, the dependence of the contact area on the applied vacuum pressure is described by Hertzian contact theory [50], expressed as

$$a = C\left(\frac{3pR^3}{E}\right)^{1/3}, \tag{3}$$

where a is the contact radius, E is the Young's modulus, R is the sphere's outer radius, and p is the confinement pressure exerted by the plastic skin. This relationship demonstrates that variations in pressure correspond to changes in contact radius and, consequently, in the global stiffness of the material.

In the real structured fabric, each unit cell (Fig. 1(c)) exhibits more than the four contact points considered in the simplified model. Furthermore, under vacuum conditions, lattice rearrangements modify both the number and configuration of these contacts, leading to changes in the effective macroscopic stiffness. Rather than representing an empirical fitting parameter, the factor C in Eq. (3) is introduced as an effective microstructural quantity accounting for the average number of simultaneous Hertzian contacts established between neighbouring unit cells under confinement. As the vacuum pressure increases, neighbouring octahedral spheres locally rearrange, allowing multiple truss members to come into contact simultaneously. Assuming that these individual contacts experience comparable local loading conditions, their normal contact stiffnesses act approximately in parallel, resulting in an equivalent contact

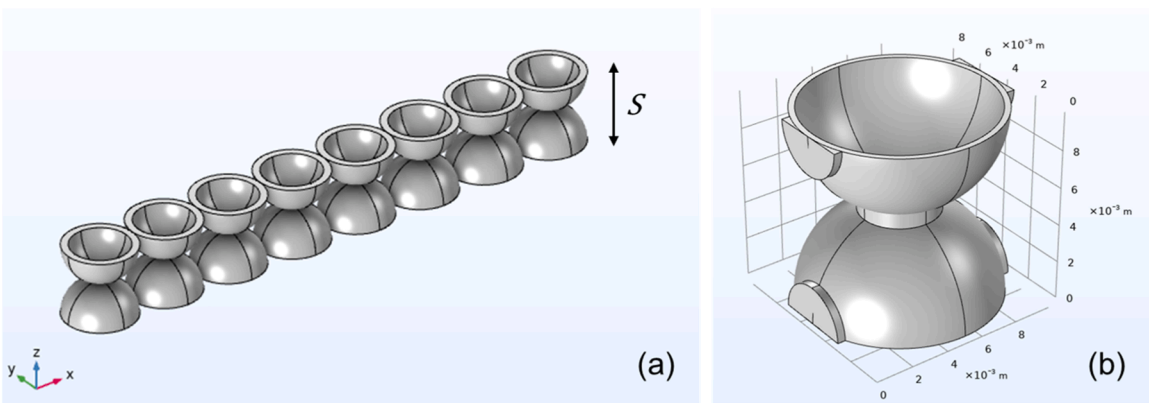

Fig. 6. Simplified tuneable structured fabrics model used for simulations. (a) domain of the infinite beam with Floquet BCs applied to the faces perpendicular to the z-axis, (b) schematic of the unit cell domain showing magnified contact areas.

stiffness proportional to the average contact multiplicity. Consequently, the contact radius is scaled by the factor C, which provides a homogenised description of the evolving contact network while preserving the computational efficiency of the periodic model. This interpretation is consistent with previous studies on jammed architected fabrics [11], which showed that the effective mechanical response of jammed systems is governed primarily by the topology of the contact network, whereas the intrinsic material properties of the individual particles have a comparatively smaller influence provided that the particles remain sufficiently rigid. Accordingly, the factor C is interpreted here as an average contact multiplicity representative of the jammed microstructure rather than as an arbitrary calibration parameter. This approach aims to homogenise the slightly heterogeneous mechanical response arising from discrete and non-uniform contact configurations.

Material properties, meshing, and parametric considerations were incorporated as follows. According to the supplier's data, the Nylon PA12 used for the realisation of the 3D-printed structured fabrics has a Young's modulus of approximately 1800 MPa, a nominal Poisson's ratio of 0.43–0.47, and a density of about 1010 kg/m^3. To achieve the same effective stiffness and mass properties of the octahedral spheres, the material parameters of the hollow spheres were adjusted based on the PA12 reference values. To account for the combined effects of manufacturing-induced material degradation and the geometric differences of the structured fabric elements, the numerical model adopted an effective Young's modulus of 900 MPa, a Poisson's ratio of 0.45, and an effective density of 192 kg/m^3. In particular, the effective structural density was determined by averaging the measured mass of individual spheres and dividing it by the corresponding sphere volume computed in COMSOL Multiphysics. The effective Young's modulus was obtained by averaging the results of multiple quasi-static compression tests performed on single chain-mail grains using a Tinius Olsen testing machine. Meshing and the related element sizing was determined automatically in COMSOL Multiphysics using the "normal" setting in "general physics" with second-order free tetrahedral elements generating 6723 elements per unit cell. Mesh convergence was manually verified by incrementally refining the mesh from "very coarse" to "very fine". The "normal" setting was chosen as the optimal balance between accuracy and computational cost, since the subsequent finer refinement yielded a change in cut-off frequencies below the accuracy threshold.

4.2. Dispersion curves

Shown in Fig. 7 are the dispersion curves computed in COMSOL Multiphysics using Floquet BCs for vacuum pressures of 20 kPa and 80 kPa. They are plotted as wavenumber versus frequency and represented by red dots. As previously noted, increasing the vacuum pressure leads not only to a larger contact area between adjacent spheres but also to an increase in the overall number of contacts. To account for this effect, the contact multiplicity factor C in Eq. (3) was set to four in the following simulations, corresponding to an average of approximately sixteen contact points per sphere under confinement. This value provides a homogenised representation of the jammed contact network and is consistent with the average number of contacts reported in [11].

The dispersion curves were computed over a frequency range up to 10 kHz by selecting the first 15 eigenfrequencies and were overlaid to the corresponding experimental ones (black dots) presented in Section 3.3, which were obtained using the correlation technique up to 5 kHz. The Floquet wavenumber was swept in the z-direction within the range $\left[0,\ \frac{\pi}{S}\right]$, where the parameter S was set to 10 mm and consequently the Brillouin zone is $[0,\ 314]$ rad/m, corresponding to the smallest repeatable domain, to avoid band folding. It is worth noting that the built-in Floquet BCs in COMSOL Multiphysics restrict the analysis to real-valued wavenumbers. In addition, damping was not included in the model; therefore, the numerical dispersion curves represent purely undamped propagating wave modes. This inherent limitation of the numerical framework, which yields only real wavenumbers, further supports the adoption of a correlation technique formulated in terms of real wavenumbers and thus tailored to propagating waves.

Initially, the dispersion curves computed at a vacuum pressure of 20 kPa are considered (see Fig. 7(a)). Within the investigated frequency range, the simplified model predicts the presence of three zero-order wave modes that propagate at all frequencies, alongside several cut-off modes. The results also reveal multiple mode crossings and a mode veering near the branch that exhibits a cut-

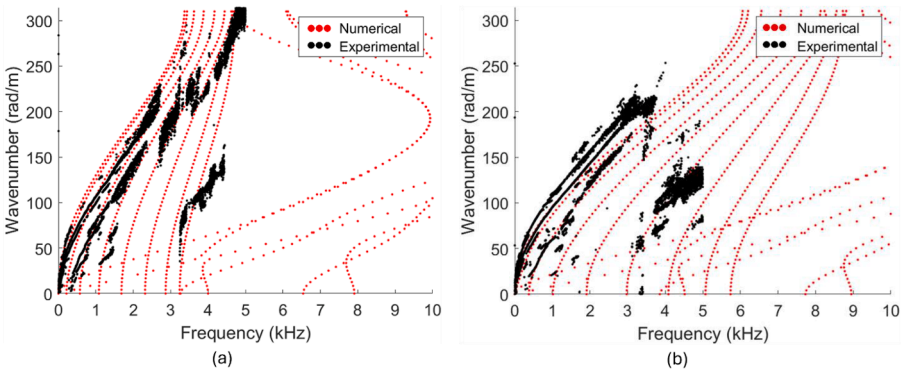

Fig. 7. Comparison between numerical and experimental dispersion curves for the in vacuo tuneable structured fabrics. The numerical solutions (in red) are implemented on COMSOL Multiphysics through the Floquet BC method, while the experimental ones (in black) via the correlation technique. (a) Dispersion curves for a vacuum pressure of 20 kPa, and (b) 80 kPa.

off frequency of approximately 4 kHz. Mode veering is a characteristic dispersion phenomenon in which, in the proximity of a critical frequency, two dispersion branches with slopes of the same sign (same direction of the energy velocity) abruptly veer apart rather than crossing, exchanging their trajectories. The corresponding wave mode shapes presented in Section 4.3 confirm that the interacting modes exchange their modal characteristics after the veering point, indicating modal hybridisation caused by wave-mode interaction rather than a true crossing. This interpretation is consistent with recent findings by Manconi et al. [51], who showed that strong wave coupling underlies mode interaction and, in periodically folded structures, may even lead to complete band-gap formation. In the present structure, although mode interaction is clearly observed, no complete band gaps develop within the investigated frequency range, suggesting that the coupling strength is insufficient to produce the locking mechanism reported in [51].

Another notable feature is the occurrence of negative group velocities. Across the full frequency range, most dispersion branches initially exhibit a positive slope before gradually transitioning to a negative slope, while a few branches cut off with a negative slope from the outset, indicating regions of negative group velocity. At higher frequencies, some branches that initially propagate with a positive slope abruptly transition to a negative slope at a wavenumber of about 200 rad/m, resulting in backward propagation. Although a universally accepted interpretation of negative group velocity remains lacking in the literature, it is generally understood that it cannot occur in isolation; rather, it is accompanied by a positive group velocity component, forming a composite wave group that propagates forward while experiencing attenuation [52–56]. This phenomenon warrants further investigation in future work.

Similar observations can be made for the numerical dispersion curves shown in Fig. 7(b). For the 80 kPa case, cut-off frequencies shift toward higher values, reflecting structural stiffening and providing additional confidence in the adopted contact modeling approach. While the experimental and numerical dispersion curves match closely in shape, the numerical model slightly overestimates structural stiffness. At both pressure levels, the numerical dispersion curves and experimental data show good qualitative agreement at low frequencies (below approximately 3 kHz), supporting the underlying simplifying assumptions. The first few branches are consistently captured, with comparable slope and curvature. Discrepancies arise at higher frequencies (above 3 kHz), where experimental data are more scattered, possibly due to wave attenuation, measurement noise, and mode superposition. Notably, the correlation technique identifies only the dominant excited wavenumbers at each frequency, whereas the numerical model accounts for all elastic waves that can propagate within the structure. Additional discrepancies originate from the simplifying assumptions adopted in the numerical model, including the representation of the jammed fabric as an equivalent periodic medium with homogeneous contact properties, local contact heterogeneity, manufacturing imperfections, and the stiffness contribution of the enclosing membrane. These simplifications are expected to have a progressively larger influence at higher frequencies, where the response becomes increasingly sensitive to the local microstructure.

Finally, as expected, increasing the confining pressure from 20 kPa to 80 kPa induces an overall upward shift of the dispersion branches in frequency for a given wavenumber, indicating an increase in structural stiffness as the plastic skin tightens around the structured fabrics. At 80 kPa, the model predicts that the contact radius is roughly twice that at 20 kPa, further highlighting the strong pressure-dependent tunability of the metamaterial's dispersion characteristics.

To provide a physical interpretation of the fundamental branches of the dispersion curves, Fig. 8 compares the dispersion curves at the confinement pressure of 20 kPa with the analytical wave solutions of an equivalent homogeneous beam derived from Euler-Bernoulli theory. Although the local mechanics of the tuneable structured fabric is governed by nonlinear Hertzian contact and interfacial friction, the macroscopic response of the system is well approximated by that of a linear, homogeneous beam. This is

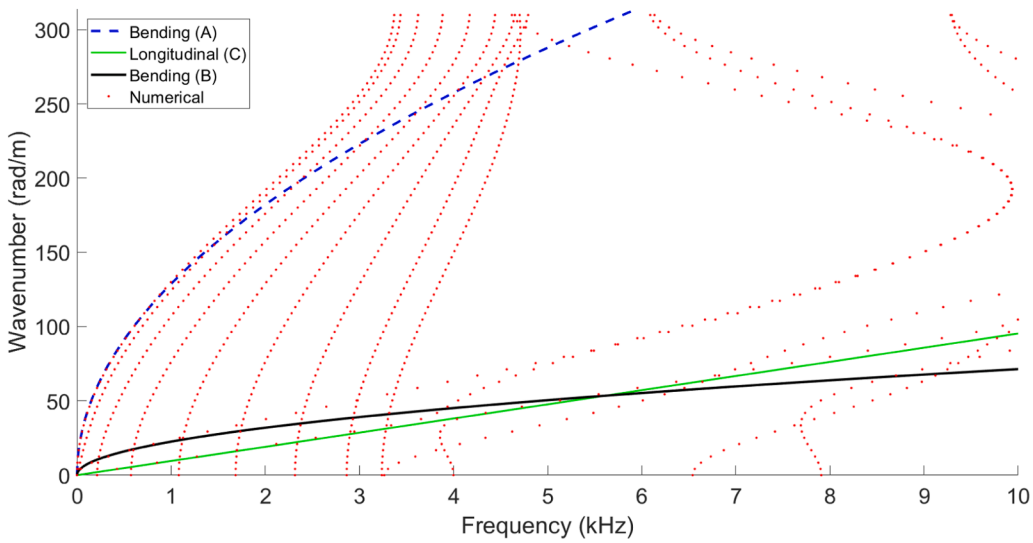

Fig. 8. Comparison of dispersion curves for the in-vacuo tuneable structured fabrics at a vacuum pressure of 20 kPa with analytical wave solutions from Euler-Bernoulli beam theory. Red dots denote the COMSOL numerical results, blue (A) and black (B) lines correspond to dispersive bending wave modes, and the green line represents the non-dispersive longitudinal wave mode (C) of an equivalent homogenous beam.

explained by the fact that the propagating wavelengths are significantly larger than the characteristic dimensions of the individual lattice elements.

The analytical solutions, namely the two zero-order bending wave modes (blue line, A, and black line, B) and the longitudinal mode (green line, C), closely match the numerical results along the positive-slope branches, up to the point where the numerical curves transition to a negative slope. The blue line indicates the bending mode along the narrower cross-sectional dimension, while the black line relates to the bending mode in the stiffer direction. The numerical longitudinal mode follows the analytical non-dispersive green curve at low frequencies, then becomes dispersive, veering around 3.8 kHz and crossing the bending wave mode (B) near 5 kHz. Both modes abruptly switch to a negative slope at a wavenumber of approximately 200 rad/m, resulting in backward propagation. To further characterize the dispersion branches, selected wave mode shapes, including the highlighted zero-order modes, are presented in the next section.

4.3. Wave mode shapes

In this section, a selection of wave mode shapes is presented to assess the significance of the different dispersion branches and to elucidate the behavior of waves propagating in the in-vacuo structured fabric. To facilitate their identification, a portion of the dispersion curves corresponding to the vacuum level of 20 kPa is shown in Fig. 9(a). The wave modes, labelled from A to F, are associated with the corresponding mode shapes depicted in Fig. 9(b). The mode shapes are illustrated by superimposing the deformed configuration of the waveguide domain, which reflects the structural periodicity, onto a reference configuration.

As noted earlier, within this frequency range the model predicts three zero-order wave modes that propagate at all frequencies: two bending modes (A and B) and one longitudinal mode (C). The flexural mode A clearly show rigid body motion in the y direction, whereas mode B displays rigid displacement along the x direction. The longitudinal mode C instead shows a rigid displacement along the wave propagation direction, z. Eight higher-order bending modes are also identified. The first three, labelled D, E, and F, follow a consistent pattern characterized by an increasing number of modal nodes. For instance, mode D represents the higher-order counterpart of the bending mode A. In this case, the displacements are out of phase, and a nodal point appears at the centre of the cross-

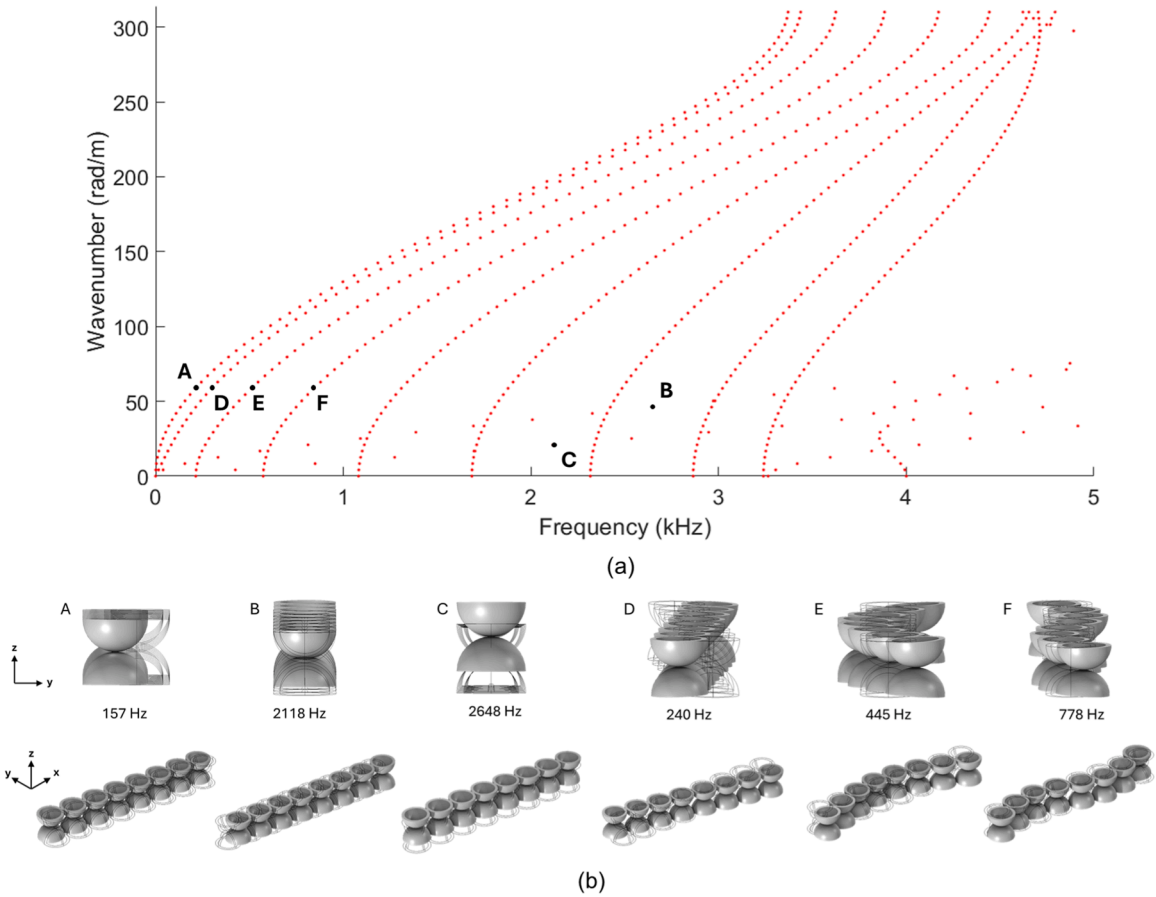

Fig. 9. Wave mode shapes of the in-vacuo structured fabrics. (a) portion of numerical dispersion curves for a vacuum pressure of 20 kPa, and (b) pictorial of selected wave mode shapes.

section, indicating second-order bending. Two additional wave modes with cut-off frequencies of approximately 3.2 kHz and 4 kHz are observed. Notably, the mode cutting off at 4 kHz with a negative slope appears as a higher-order longitudinal mode before transitioning into a bending mode after veering.

The evolution of the wave mode shapes with frequency was also investigated, revealing that they remain consistent along both the positive- and negative-slope branches. Mode veering between the zero-order longitudinal mode C and the mode cutting off at 4 kHz is confirmed, with the corresponding mode shapes exchanging characteristics beyond the veering point. Within the veering region, however, both modes assume a more complex, non-recognisable shape that deviate from their typical patterns.

5. Conclusion

This study presented a preliminary investigation of wave propagation in beam-like, in-vacuo structured fabrics under different confinement pressures. A simplified one-dimensional wave finite element model of these structures was implemented in COMSOL Multiphysics, employing the Floquet BC method combined with Hertzian contact theory. Dispersion curves were computed for vacuum pressures of 20 kPa and 80 kPa and subsequently compared with corresponding experimental measurements. The numerical model successfully reproduced the main experimental dispersion features for both pressure conditions, with small discrepancies at higher frequencies attributed to wave attenuation, measurement noise, and modelling simplifications.

Overall, the combined dispersion and wave mode shape analyses provide a comprehensive understanding of wave propagation in the in-vacuo structured fabric and confirm the validity of the adopted modelling strategy. The numerical dispersion curves reproduce the principal features of the experimental measurements, particularly at low frequencies, and accurately capture key features such as cut-off modes, mode crossing, mode veering, and regions of negative group velocity. The comparison with the equivalent Euler–Bernoulli beam further clarifies the physical nature of the fundamental branches, enabling a clear identification of bending and longitudinal wave modes and their evolution with frequency. The examination of wave mode shapes corroborates these findings, revealing consistent modal characteristics along the branches and confirming the exchange of modal features within the veering region. Importantly, the observed upward shift of the dispersion curves with increasing confinement pressure demonstrates the strong pressure-dependent tunability of the metamaterial, linking contact mechanics to its global dynamic response. Together, these results establish a coherent framework for interpreting the complex wave phenomena governing the system and highlight the effectiveness of the proposed approach in capturing both qualitative trends and the underlying physical mechanisms.

The results demonstrate that vacuum-controlled structured fabrics exhibit highly tuneable wave dynamics. Most importantly, they show that this behaviour can be predicted using a simplified model derived from Hertzian contact theory, with modifications incorporated to account for contact multiplicity. Increasing the confinement pressure enhances the overall stiffness of the structure, resulting in a shift of the dispersion branches toward higher frequencies. Notably, the dispersion analysis revealed the occurrence of negative group velocities, indicating the coexistence of forward- and backward-propagating waves. Wave mode shape analysis confirmed the presence of multiple bending and longitudinal modes, with the forward-propagating branches aligning closely with classical beam theory predictions. These findings provide fundamental insight into tuneable wave dynamics in adaptive structures and highlight promising directions for future research. In particular, since the operative wavelengths are significantly larger than the characteristic grain size of the material, the in-vacuo structured fabric effectively behaves as a homogeneous tuneable structure. Although its underlying architecture remains discrete, contact-based, and inherently nonlinear, its macroscopic response remains predictable and highly tuneable. Consequently, within the frequency and excitation amplitude ranges investigated in this study, the material can be approximated as an equivalent linear homogeneous waveguide with pressure-dependent effective properties. This allows the in-vacuo structured fabric to function as a programmable material whose effective mechanical properties are controlled solely by the confinement pressure within the airtight membrane, providing a versatile platform for the development of adaptive metamaterials and advanced vibration control systems.

CRediT authorship contribution statement

Davide Raffaele: Writing – review & editing, Writing – original draft, Software, Methodology, Investigation, Funding acquisition, Formal analysis, Data curation, Conceptualization. **Emiliano Rustighi:** Writing – review & editing, Writing – original draft, Supervision, Resources, Project administration, Methodology, Conceptualization. **Paolo Gardonio:** Writing – review & editing, Supervision, Methodology, Conceptualization. **Ciro Malacarne:** Writing – review & editing, Validation, Resources, Investigation. **Matteo Perini:** Writing – review & editing, Validation, Resources, Investigation.

Declaration of competing interest

The authors declare that they have no known competing financial interests or personal relationships that could have appeared to influence the work reported in this paper.

Acknowledgements

This work was funded by the European Union - NextGenerationEU, under the Italian Ministry of University and Research (MUR) PNRR Mission 4 Component 2 – PRIN 2022 (Project Code: 20223×5S37, CUP: E53D23002640006).

Data availability

Data will be made available on request.

References

[1] E. Montgomery-Liljeroth, S. Schievano, G. Burriesci, Elastic properties of 2D auxetic honeycomb structures-a review, Appl. Mater. Today 30 (2023) 101722, https://doi.org/10.1016/j.apmt.2022.101722.

[2] M. Gholikord, E. Etemadi, M. Imani, M. Hosseinabadi, H. Hu, Design and analysis of novel negative stiffness structures with significant energy absorption, Thin-Walled Struct. 181 (2022) 110137, https://doi.org/10.1016/j.tws.2022.110137.

[3] P. Ma, H. Wang, X. Fan, C. Hou, Design of metamaterial for broadband sound absorption through double resonances, J. Vib. Acoust. 146 (2024) 041004, https://doi.org/10.1115/1.4066653.

[4] P. Yan, H. Huang, M. Meloni, B. Li, J. Cai, Mechanical properties inside origami-inspired structures: an overview, Appl. Mech. Rev. 77 (2025) 011001, https://doi.org/10.1115/1.4066566.

[5] D. Misseroni, P.P. Pratapa, K. Liu, B. Kresling, Y. Chen, C. Daraio, G.H. Paulino, Origami engineering, Nat. Rev. Methods Primers 4 (2024) 40, https://doi.org/10.1038/s43586-024-00313-7.

[6] E. Rustighi, P. Gardonio, S. Baldini, C. Malacarne, M. Perini, Vibration response of in-vacuo tuneable structured fabrics, J. Vib. Control 31 (2025) 4–23, https://doi.org/10.1177/10775463241245251.

[7] P. Gardonio, E. Rustighi, S. Baldini, C. Malacarne, M. Perini, In-vacuo adaptive beam element for vibration control, Mech. Syst. Signal Process. 224 (2025) 112089, https://doi.org/10.1016/j.ymssp.2024.112089.

[8] P. Gardonio, L. Ortis, E. Rustighi, C. Malacarne, M. Perini, Multi-resonant TVA formed by a tree of deflated composite beams with core structured fabrics, Smart Mater. Struct. 34 (2025) 015039, https://doi.org/10.1088/1361-665X/ad9c07.

[9] I. Gibson, D. Rosen, B. Stucker, M. Khorasani, Direct Digital Manufacturing, in: I. Gibson, D. Rosen, B. Stucker, M. Khorasani (Eds.), Additive Manufacturing Technologies, third ed., Springer, New York, 2021, pp. 525–554, https://doi.org/10.1007/978-3-030-56127-7.

[10] X. Chen, L.W. Taylor, L.J. Tsai, An overview on fabrication of three-dimensional woven textile preforms for composites, Text. Res. J. 81 (2011) 932–944, https://doi.org/10.1177/0040517510392471.

[11] Y. Wang, L. Li, D. Hofmann, J.E. Andrade, C. Daraio, Structured fabrics with tunable mechanical properties, Nature 596 (2021) 238–243, https://doi.org/10.1038/s41586-021-03698-7.

[12] L. Orgéas, Chain-mail fabric stiffens under confining pressure, Nature 596 (2021) 196–197, https://doi.org/10.1038/d41586-021-02116-2.

[13] Y. Jiang, D. Chen, C. Liu, J. Li, Chain-like granular jamming: a novel stiffness-programmable mechanism for soft robotics, Soft Robot. 6 (2019) 118–132, https://doi.org/10.1089/soro.2018.0005.

[14] R.P. Behringer, B. Chakraborty, The physics of jamming for granular materials: a review, Rep. Prog. Phys. 82 (2019) 012601, https://doi.org/10.1088/1361-6633/aadc3c.

[15] A.J. Liu, S.R. Nagel, Jamming and Rheology: Constrained Dynamics on Microscopic and Macroscopic Scales, first ed., CRC Press, 2001 https://doi.org/10.1201/9781482268171.

[16] A.J. Liu, S.R. Nagel, The jamming transition and the marginally jammed solid, Annu. Rev. Condens. Matter Phys. 1 (2010) 347–369, https://doi.org/10.1146/annurev-conmatphys-070909-104045.

[17] T.S. Majmudar, R.P. Behringer, Contact force measurements and stress-induced anisotropy in granular materials, Nature 435 (2005) 1079–1082, https://doi.org/10.1038/nature03805.

[18] A.V. Dyskin, Y. Estrin, A.J. Kanel-Belov, E. Pasternak, A new concept in design of materials and structures: assemblies of interlocked tetrahedron-shaped elements, Scr. Mater. 44 (2001) 2689–2694, https://doi.org/10.1016/s1359-6462(01)00968-x.

[19] J.P. Den Hartog, Mechanical Vibrations, fourth ed., McGraw-Hill, New York, 1986.

[20] E. Rustighi, M.J. Brennan, B.R. Mace, A shape memory alloy adaptive tuned vibration absorber: design and implementation, Smart Mater. Struct. 14 (2005) 19–28, https://doi.org/10.1088/0964-1726/14/1/002.

[21] E. Rustighi, D.F. Ledezma-Ramirez, P.E. Tapia-Gonzalez, N. Ferguson, A. Zakaria, Modelling and experimental characterisation of a compressional adaptive magnetorheological elastomer isolator, J. Vib. Control 28 (2022) 3093–3107, https://doi.org/10.1177/10775463211025336.

[22] N. Boechler, L. Yang, G. Theocharis, P.G. Kevrekidis, C. Daraio, Tunable vibrational band gaps in one-dimensional diatomic granular crystals with three-particle unit cells, J. Appl. Phys. 109 (2011) 074906, https://doi.org/10.1063/1.3556455.

[23] M. Manjunath, A.P. Awasthi, P.H. Geubelle, Plane wave propagation in 2D and 3D monodisperse periodic granular media, Granul. Matter. 16 (2014) 141–150, https://doi.org/10.1007/s10035-013-0475-z.

[24] F. Göncü, S. Luding, K. Bertoldi, Exploiting pattern transformation to tune phononic band gaps in a two-dimensional granular crystal, J. Acoust. Soc. Am. 131 (2012) EL475–EL480, https://doi.org/10.1121/1.4718384.

[25] L. Gavrić, Computation of propagative waves in free rail using a finite element technique, J. Sound Vib. 185 (1995) 531–543, https://doi.org/10.1006/jsvi.1995.0398.

[26] T. Hayashi, W.J. Song, J.L. Rose, Guided wave dispersion curves for a bar with an arbitrary cross-section, a rod and rail example, Ultrasonics 41 (2003) 175–183, https://doi.org/10.1016/S0041-624X(03)00097-0.

[27] V. Damljanović, R.L. Weaver, Forced response of a cylindrical waveguide with simulation of the wavenumber extraction problem, J. Acoust. Soc. Am. 115 (2004) 1582–1591, https://doi.org/10.1121/1.1675818.

[28] B.C. Lee, W.J. Staszewski, Modelling of Lamb waves for damage detection in metallic structures: Part II. Wave interactions with damage, Smart Mater. Struct. 12 (2003) 815–824, https://doi.org/10.1088/0964-1726/12/5/019.

[29] M. Collet, M. Ouisse, M. Ruzzene, M.N. Ichchou, Floquet–Bloch decomposition for the computation of dispersion of two-dimensional periodic, damped mechanical systems, Int. J. Solids Struct. 48 (2011) 2837–2848, https://doi.org/10.1016/j.ijsolstr.2011.06.002.

[30] T.C. Wu, T.T. Wu, J.C. Hsu, Waveguiding and frequency selection of Lamb waves in a plate with a periodic stubbed surface, Phys. Rev. B—Condens. Matter Mater. Phys. 79 (2009) 104306, https://doi.org/10.1103/PhysRevB.79.104306.

[31] C. Hakoda, J. Rose, P. Shokouhi, C. Lissenden, Using Floquet periodicity to easily calculate dispersion curves and wave structures of homogeneous waveguides, AIP Conf. Proc. 1949 (2018) 020016, https://doi.org/10.1063/1.5031513.

[32] COMSOL Multiphysics® v. 6.3, Stockholm, Sweden, 2024. https://www.comsol.com.

[33] D. Alleyne, P. Cawley, A two-dimensional Fourier transform method for the measurement of propagating multimode signals, J. Acoust. Soc. Am. 89 (1991) 1159–1168, https://doi.org/10.1121/1.400530.

[34] K. Grosh, E.G. Williams, Complex wave-number decomposition of structural vibrations, J. Acoust. Soc. Am. 93 (1993) 836–848, https://doi.org/10.1121/1.405445.

[35] J.G. McDaniel, W.S. Shepard Jr, Estimation of structural wave numbers from spatially sparse response measurements, J. Acoust. Soc. Am. 108 (2000) 1674–1682, https://doi.org/10.1121/1.1310668.

[36] M. Kley, C. Valle, L.J. Jacobs, J. Qu, J. Jarzynski, Development of dispersion curves for two-layered cylinders using laser ultrasonics, J. Acoust. Soc. Am. 106 (1999) 582–588, https://doi.org/10.1121/1.427135.

[37] A. Santoni, S. Schoenwald, B. Van Damme, P. Fausti, Determination of the elastic and stiffness characteristics of cross-laminated timber plates from flexural wave velocity measurements, J. Sound Vib. 400 (2017) 387–401, https://doi.org/10.1016/j.jsv.2017.04.018.

[38] I. Roelens, F. Nuytten, I. Bosmans, G. Vermeir, In situ measurement of the stiffness properties of building components, Appl. Acoust. 52 (1997) 289–309, https://doi.org/10.1016/S0003-682X(97)00032-7.
[39] B. Zhang, T.P. Waters, B.R. Mace, Identifying joints from measured reflection coefficients in beam-like structures with application to a pipe support, Mech. Syst. Signal Process. 24 (2010) 784–795, https://doi.org/10.1016/j.ymssp.2009.10.023.
[40] N.S. Ferguson, C.R. Halkyard, B.R. Mace, K.H. Heron, The estimation of wavenumbers in two-dimensional structures, in: ISMA International Conference on Noise and Vibration, Leuven 16-18 September 2002, 2002, pp. 799–806.
[41] E. El Masri, N. Ferguson, T. Waters, Wave propagation and scattering in reinforced concrete beams, J. Acoust. Soc. Am. 146 (2019) 3283–3294, https://doi.org/10.1121/1.5131644.
[42] M.R. Souza, D. Beli, N.S. Ferguson, J.R.D.F. Arruda, A.T. Fabro, A Bayesian approach for wavenumber identification of metamaterial beams possessing variability, Mech. Syst. Signal Process. 135 (2020) 106437, https://doi.org/10.1016/j.ymssp.2019.106437.
[43] C. Cai, W.S. Tey, J. Chen, W. Zhu, X. Liu, T. Liu, L. Zhao, K. Zhou, Comparative study on 3D printing of polyamide 12 by selective laser sintering and multi jet fusion, J. Mater. Process. Technol. 288 (2021) 116882, https://doi.org/10.1016/j.jmatprotec.2020.116882.
[44] S. Baldini, D. Raffaele, P. Gardonio, E. Rustighi, C. Malacarne, M. Perini, The effect of unit particle geometry on in-vacuo structured fabrics flexural vibration, J. Vib. Acoust. 148 (2026) 021007, https://doi.org/10.1115/1.4070374.
[45] M. Schroeder, Synthesis of low-peak-factor signals and binary sequences with low autocorrelation (Corresp.), IEEE Trans. Inf. Theory 16 (1970) 85–89, https://doi.org/10.1109/TIT.1970.1054411.
[46] J. Schoukens, R. Pintelon, E. Van Der Ouderaa, J. Renneboog, Survey of excitation signals for FFT based signal analyzers, IEEE Trans. Instrum. Meas. 37 (1988) 342–352, https://doi.org/10.1109/19.7453.
[47] M.N. Ichchou, J. Berthaut, M. Collet, Multi-mode wave propagation in ribbed plates: Part I, wavenumber-space characteristics, Int. J. Solids Struct. 45 (2008) 1179–1195, https://doi.org/10.1016/j.ijsolstr.2007.09.032.
[48] L. Brillouin, Wave Propagation in Periodic Structures: Electric Filters and Crystal Lattices, McGraw-Hill, New York, 1946.
[49] E. Rustighi, D. Raffaele, P. Gardonio, C. Malacarne, M. Perini, A modeling study of elastic properties of structured fabrics under vacuum pressure, in: ECCOMAS Proceedia, Proceedings of the XI ECCOMAS Thematic Conference on Smart Structures and Materials (SMART 2025), Linz, Austria, 1-3 July 2025, 2025.
[50] V.L. Popov, Contact Mechanics and Friction, Second ed., Springer-Verlag, Berlin, 2017 https://doi.org/10.1007/978-3-662-53081-8.
[51] E. Manconi, F. Dall'Olio, M. Riboli, A. Zippo, F. Tatar, Contradirectional coupling and complete band gap formation in periodically folded beams and plates, J. Sound Vib. 636 (2026) 119799, https://doi.org/10.1016/j.jsv.2026.119799.
[52] J. Lei, W. Li, Q. Qiao, L. Zhang, J. Lin, Negative group velocity characteristics of spoof surface plasmon polaritons, AIP Adv. 13 (2023) 035214, https://doi.org/10.1063/5.0141185.
[53] J. Lee, Analysis of the interaction between torsion wave and phononic crystal in pipes, AIP Adv. 13 (2023) 105032, https://doi.org/10.1063/5.0160973.
[54] K. Tamm, T. Peets, J. Engelbrecht, D. Kartofelev, Negative group velocity in solids, Wave Motion 71 (2017) 127–138, https://doi.org/10.1016/j.wavemoti.2016.04.010.
[55] P.L. Marston, Negative group velocity Lamb waves on plates and applications to the scattering of sound by shells, J. Acoust. Soc. Am. 113 (2003) 2659–2662, https://doi.org/10.1121/1.1564021.
[56] H. Cui, W. Lin, H. Zhang, X. Wang, J. Trevelyan, Backward waves with double zero-group-velocity points in a liquid-filled pipe, J. Acoust. Soc. Am. 139 (2016) 1179–1194, https://doi.org/10.1121/1.4944046.